Pancreatic nerve electrostimulation inhibits recent-onset autoimmune diabetes

Mélanie Guyot, Thomas Simon, Franck Ceppo, Clara Panzolini, Alice Guyon, Julien Lavergne, Emilie Murris, Douglas Daoudlarian, Romain Brusini, Hadi Zarif, et al.

Pancreatic nerve electrostimulation inhibits recent onset autoimmune diabetes

Mélanie Guyot[1], Franck Ceppo[1], Thomas Simon[1], Alice Guyon[1], Clara Panzolini[1], Emilie Murris[1], Douglas Daoudlarian[1], Romain Brusini[1], Hadi Zarif[1], Sophie Abelanet[1], Sandrine Hugues-Ascery[3], Jean-Louis Divoux[4], Stephen J. Lewis[5], Arun Sridhar[6], Nicolas Glaichenhaus[1] and Philippe Blancou[1]

[1]Université Côte d'Azur, CNRS, INSERM, Institut de Pharmacologie Moléculaire et Cellulaire, Valbonne, France

[3]E-PHY-SCIENCE, Valbonne, France

[4]AXONIC, Vallauris, France.

[5]Departments of Pediatrics and Pharmacology, School of Medicine, Case Western Reserve University, Cleveland, OH, USA

[6]Galvani Bioelectronics, Stevenage, U.K.

Key words: electrostimulation, autoimmune diabetes, T-cells, cross-presentation, leukocyte migration, inflammation

Total word counts: 1593 words

Electrical modulation of peripheral nerves has been proposed as a novel approach to treat immune-mediated inflammatory diseases (IMIDs)[1]. Type-1 diabetes (T1D) is an autoimmune disease that results from the destruction of insulin-producing pancreatic β cells by autoreactive T lymphocytes following their activation in pancreatic draining lymph nodes (LNs)[2]. The sympathetic nervous system inhibits inflammation via binding of noradrenaline or adrenaline to β_2-adrenergic receptors (ARs) expressed on immune cells[3]. Since LNs are innervated by sympathetic nerves, we hypothesized that pancreatic nerve electrical stimulation (PNES) may inhibit local inflammation and T1D progression. Here we have developed a minimally invasive surgical procedure for long-term implantation of micro-cuffs electrodes onto the nerve that projects to pancreatic draining LNs. When applied to recently diabetic Non-Obese-Diabetic (NOD) mice, PNES inhibited insulitis and T1D progression with minimal bystander tissue effects by inhibiting the migration of pathogenic effector T lymphocytes from pancreatic draining LNs to pancreatic islets. Our data provide a rationale for the use of bio-electronic medicine as a potential treatment modality for T1D.

Little is known about the nerves that project to the pancreas in mice. Gross anatomy of the pancreatic region showed that the superior mesenteric artery branching from the inferior vena cava is associated with a 50 μm-diameter nerve-like structure (**Suppl. Fig. 1a**) and supplied blood to the pancreas head and neck (**Suppl. Fig. 1b**). To confirm that this structure was a nerve and to identify the innervated tissues, we placed a hook electrode onto it and a recording electrode on visceral tissues. Evoked compound action potentials (CAPs) occurred in pancreatic LNs and pancreas head but not in liver when electrostimulation was applied (**Suppl. Fig. 2**). Pancreatic nerve-like structures expressed tyrosine hydroxylase (TH) demonstrating the presence of catecholaminergic fibers (**Fig. 1a**). In agreement with the known ability of the SNS to induce vasoconstriction, high frequency and amplitude (20 Hz, 1 mA)

electrical stimulation of the pancreatic nerve reduced pancreatic blood flow using laser speckle perfusion imager (**Fig. 1b**). Light-sheet-based fluorescent imaging of TH-stained LNs showed a high-density network of catecholaminergic fibers showing that the pancreatic nerve did not only project to the pancreas itself, but also to the LNs that drained this gland (**Fig. 1c**). To characterize the electrophysiological properties of the pancreatic nerve fibers, we used fluorescent reporter tdTomato$^{TH\text{-}Cre}$ transgenic mice carrying the tdTomato fluorescent protein gene downstream of the tyrosine hydroxylase (TH) gene promoter. Red fluorescence axons were readily detected in both the pancreatic nerve (**Suppl. Fig. 3a**) and the pancreatic LN medulla zone (**Suppl. Fig. 3b**). To confirm that the pancreatic nerve projected to the pancreatic LN, we placed these red fluorescent axons of the pancreatic nerve into a suction electrode and recorded field action potentials (FAPs) with a microelectrode. FAPs were readily detected when pancreatic nerve electrical stimulation (PNES) was above 400 µA (**Fig. 1d**). FAPs were inhibited by tetrodotoxin (TTX) confirming that they resulted from neuronal activity (**Suppl. Fig. 4a**). Nerve conduction velocity was 0.5 ± 0.26 m/s at 25 °C (n = 4) suggesting that axons were unmyelinated[4].

Should PNES be considered as a therapeutic treatment, electrical parameters need be optimized to minimize bystander tissue damage and short-term alterations in pancreatic blood flow and glycemia, while allowing release of therapeutic levels of neurotransmitters. After testing various electrical stimulation parameters, we found that a frequency of 10 Hz and an amplitude of 450 µA increased noradrenaline levels in pancreatic LNs (**Fig. 1e)** without altering pancreatic blood flow (**Fig. 1b**) or glycemia (**Suppl. Fig. 5**). Furthermore, these parameters did not induce exhaustion of axonal excitability (**Suppl. Fig. 4b, 4c**) therefore preserving therapeutic efficacy.

We then investigated whether PNES could impact secretion of pro-inflammatory cytokines, immune cell trafficking and antigen cross-priming in the pancreatic draining LNs of

non-diabetic prone mice. Because anesthetics interfere with immunity[5], we developed a minimally invasive surgical procedure for sustainable implantation of micro-cuffs electrodes onto the pancreatic nerve allowing studies to be conducted on conscious animals. Compared to sham-stimulated mice in which a cuff was implanted but electrical stimulation was not applied, PNES mice exhibited higher numbers of T and B-lymphocytes in pancreatic draining but not in non-draining LNs (**Fig. 2a**, **Suppl. Fig. 6a-c**). No alterations in the frequency of myeloid cell types were observed **Suppl. Fig. 6d**). One session of PNES reduced LPS-induced pro-inflammatory cytokine mRNA levels in pancreatic LNs but not in spleen (**Fig. 2b**). We next assessed the impact of electrostimulation on the ability of dendritic cells (DC) to cross-prime CD8+ T cells taking advantage of the RIP-OVA mice in which ovalbumin (OVA) is exclusively expressed in β-islets. In this model, naïve OVA-specific CD8 T (OT-1) cells transferred in these mice spontaneously proliferate as consequence of OVA antigen presentation by DC in pancreatic lymph nodes. When applied over a 4-day period, PNES inhibited pancreatic auto-antigen cross-priming as shown by reduced proliferation of adoptively transferred islet-specific $CD8^+$ T cells (**Fig. 2c**). In agreement with a critical role of noradrenaline, the effects of PNES on both immune cell accumulation and LPS-induced pro-inflammatory cytokine mRNA production were abolished in mice deficient in β_2-AR ($ADRB2^{ko}$) (**Fig. 2a**, **2b**). Likewise, administration of the β_1/ β_2-AR antagonist propranolol showed that the inhibitory effect of PNES on auto-antigen cross-priming was β-AR-dependent (**Fig. 2c**).

We next investigated the impact of PNES on T1D progression in NOD mice that spontaneously develop autoimmune diabetes between 3 and 6 months of age. Once diagnosed with diabetes, NOD mice were implanted with a micro-cuff electrode onto the pancreatic nerve and PNES was applied one day later three times a day for 6 weeks (**Fig. 3a**). Mice returned to normoglycemia after surgery, a phenomenon that was likely due to the anti-inflammatory effect of anesthetics[6,7]. However, while glycemia started to increase again in sham stimulated mice

resulting in full-blown diabetes, it remained below 150 mg/ml in PNES mice (**Fig. 3b**). To investigate the underlying mechanisms, we took advantage of a well-characterized synchronous model of diabetes in which diabetogenic T cells from NOD mice are transferred into immunodeficient syngenic NOD-SCID recipients[8]. While all (13 out of 13) sham-stimulated mice developed T1D within 4 weeks after transfer, only 55% (7 out of 13) of PNES recipients did ($p = 0.015$, **Fig. 3c**). This result showed that PNES inhibits T1D progression by acting on pathogenic effector T cells. In another set of experiments, mice were sacrificed 2 weeks after adoptive transfer and analyzed for both insulitis and number of lymphocytes in pancreatic LNs. PNES mice had 2.7-fold as many islets than sham stimulated mice (84.5 ± 20.3 versus 31.75 ± 3.6, p = 0,029) (**Fig. 3d**). In addition, the proportion of non-infiltrated islets was higher in PNES mice than in sham stimulated mice (55% versus 17.5%)(**Fig. 3d**). Furthermore, while PNES and sham-stimulated mice exhibited similar number of lymphocytes in non-draining LNs, PNES mice had 4- to 5-fold more lymphocytes in draining LNs ($29.0 \pm 12.0 \times 10^4$ versus $6.0 \pm 1.5 \times 10^4$ per mouse, $p = 0.006$), a result similar to what we also observed in C57BL/6 mice (**Fig. 3e**). Our data are compatible with a model in which PNES prevents T1D by inhibiting the migration of pathogenic effector T lymphocytes from pancreatic draining LNs to pancreatic islets.

We next investigated whether T1D inhibition could be achieved by on-demand PNES, or alternatively required persistent stimulation. Once diagnosed with diabetes, NOD mice were implanted with a micro-cuff electrode onto the pancreatic nerve and glycaemia was monitored daily for up to two months. When glycaemia exceeded 200 mg/dl, 9 to 12 PNES sessions (450 µA, 10 Hz, 2 min. duration) were applied 8 hours apart. While all mice eventually became hyperglycemic, glycaemia increased 2.25 times more slowly in PNES mice (**Fig. 3f**, **Suppl. Fig. 7**). In another set of experiments, we sacrificed mice 2 weeks after the first PNES session. PNES mice had 4.3-fold as many islets as sham stimulated mice (26.0 ± 1.5 versus 6.0 ± 1.0

per mouse, p = 0.0006) (**Fig. 3g**). Likewise, insulitis was less severe in PNES mice as demonstrated by the proportion of non-infiltrated islets (30.9% versus 15.8%).

Two clinical studies have shown that vagus nerve stimulation can be beneficial for patients with Immune-Mediated Inflammatory Diseases (IMIDs), i.e. rheumatoid arthritis[9] and Crohn's Disease[10]. However, vagus nerve electrical stimulation lacked efficacy in some patients, and had serious adverse effects, presumably because of its lower nerve fiber specificity. Indeed, the vagus nerve contains both afferent and efferent fibers, and it regulates the function of multiple organs. We have made the hypothesis that applying electrical stimulation to an exclusively efferent nerve proximal to the target organ would be both more efficient therapeutically and more specific. Here, we have identified a sympathetic nerve that projects into pancreatic LNs. Selective electrostimulation of this nerve was sufficient to completely inhibit T1D progression in both a spontaneous and an adoptive transfer models of T1D with minimal bystander effects. We also found that PNES inhibited LPS-induced production of inflammatory cytokines, antigen cross-presentation in pancreatic LN, and resulted in increased numbers of lymphocytes in pancreatic draining LN. These results are in agreement with previous studies showing an inhibitory role of β2-AR signaling on secretion of inflammatory cytokines by various myeloid cell types[3], antigen cross-presentation by dendritic cells[11] and lymphocyte egress from LN[12]. Since T1D is dependent on antigen cross-presentation, production of inflammatory cytokines and migration of autoreactive effector T cells from pancreatic LNs to pancreatic islets[2], PNES could possibly prevent T1D progression by interfering with all such pathways.

Bioelectronics medicine offers the possibility to apply on-demand treatment based on recording of physiological parameters such as glycemia. While our pilot experiments showed that on-demand PNES was not as efficient as continuous PNES at inhibiting T1D progression, technological refinements such as optimized electrical stimulation parameters or

implementation of a closed-loop system are within reach and may greatly improve its therapeutic efficacy. Thus, our study provides a rationale for the future use of bioelectronic medicine in treatment of autoimmune diabetes.

Figure Legends

Figure 1: Pancreatic nerve electrophysiological and functional characterization. (**a**) Confocal microscopy of a representative pancreatic nerve section stained for Tyrosine Hydroxylase (TH, red) or NeuroFilament (NF, blue). Scale bar = 20 μm. (**b**) Impact of PNES on surface pancreatic blood flow measured by laser speckle. Representative (of 5 mice) color-coded images (left) and quantification (right) before, during and after PNES for 15 s. Quantification was performed on the area delineated by the dotted line. (**c**). A representative image (of 3 mice) of maximal projection of a TH-stained LN, cleared and imaged by light-sheet microscopy at low magnification. Scale bar = 500 μm. (**d**) Representative recordings of fluorescent axon electrical activity in pancreatic LNs from tdTomato$^{TH\text{-}Cre}$ mice following PNES. Representative (of 4 experiments) FAPs (left) and peak amplitudes (right) as a function of PNES intensity. (**e**) Noradenaline content in pancreatic LNs following PNES (450 μA, 10 Hz, 2 min.) or sham stimulation (n = 10). Mean ± S.E.M. **, $p < 0.01$.

Figure 2: Impact of PNES on immune cell number, cytokine production and autoreactive T cell proliferation in pancreatic LNs. (**a**) Impact of PNES (450 μA, 10 Hz, 2 min duration, 3 sessions 3 hours apart) on lymphocyte numbers in pancreatic LNs. Schematic representation of the experimental protocol (left). Number of B cells, $CD4^+$ and $CD8^+$ T cells in wt (empty bars) and ADRB2^{ko} (dashed bars) mice (right). Mean ± S.E.M. of 3 experiments (n = 6-10/group). (**b**) Impact of PNES (450 μA, 10 Hz, 2 min duration) on LPS-induced TNF-α, IL-6 and IL-1β mRNA levels in spleen and pancreatic LNs. Schematic representation of the experimental protocol (left). mRNA levels in the indicated tissues in wt (empty bars) and ADRB2^{ko} (dashed bars) mice (right). Mean ± S.E.M. of 3 experiments (n = 6-8/group). (**c**) Impact of PNES (450 μA, 10 Hz, 2 min. duration, 3 sessions/day for 4 days) on autoreactive T cell proliferation. Schematic representation of the experimental protocol (left). Representative

FACS profiles of CFSE-labeled $CD8^+$ OVA-specific T cells following PNES and sham stimulation in RIP-mOVA mice (middle panel). $CD8^+$ OVA-specific T cell proliferation after PNES (normalized to sham) in mice treated (dashed bars) or not (empty bars) with propranolol (right panel). Mean ± S.E.M. of 3 experiments (n = 6-8/group). *, $p < 0.05$; **, $p < 0.01$.

Figure 3: Impact of PNES on glycaemia and insulitis in NOD mice. (**a**) Schematic representation of the experimental protocol. Recently diabetic NOD mice (glycaemia over 200 mg/dl two consecutive days) were implanted onto the pancreatic nerve with micro-cuff electrodes and PNES was applied either continuously after surgery (**b**) or on-demand when glycaemia exceeded 200mg/dl (**f**-**h**). In other experiments, NOD-SCID recipient were implanted onto the pancreatic nerve with micro-cuff electrodes, injected with 5×10^6 splenocytes from recently diabetic NOD mice and PNES was applied continuously (**c**-**e**). (**b**) Glycaemia following continuous PNES in individual mice (n = 4 / group). (**c**) Diabetes incidence in NOD-SCID mice (n = 13 / group). (**d**) Number of islets per mouse and proportion of islets exhibiting severe, mild and low immune cell infiltration two weeks after PNES. Mean ± S.E.M. (n = 4 / group). (**e**) Total number of cells (left panel) and number of B, $CD4^+$ and $CD8^+$ T cells (left panel) in pancreatic LNs two weeks after PNES. Mean ± S.E.M. (n = 5-6 / group). (**f**) Glycaemia increase following on-demand PNES. Representative mice (left panel) and mean glycaemia increase (right panel) following PNES or sham stimulation. Mean ± S.E.M. (n = 10/group). (**h**) Number of islets per mouse and proportion of islets exhibiting severe, mild and low immune cell infiltration two weeks following on-demand PNES. Mean ± S.E.M. (n = 4 / group). *, $p < 0.05$; **, $p < 0.01$; ***, $p < 0.001$.

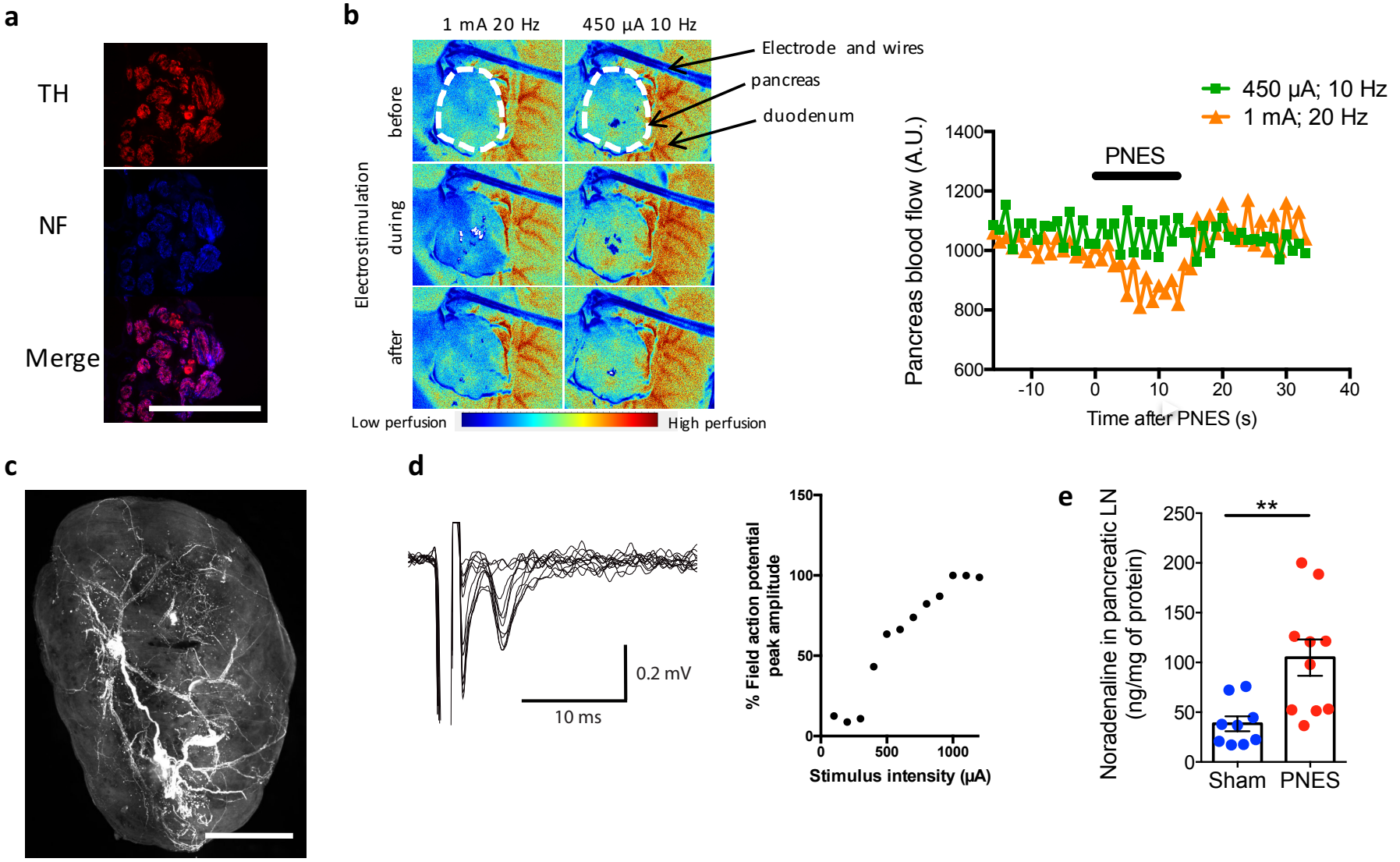
a
TH
NF
Merge
b
1 mA 20 Hz
450 µA 10 Hz
Electrostimulation
before
during
after
Electrode and wires
pancreas
duodenum
Low perfusion
High perfusion
450 µA; 10 Hz
1 mA; 20 Hz
PNES
Pancreas blood flow (A.U.)
Time after PNES (s)
c
d
0.2 mV
10 ms
% Field action potential peak amplitude
Stimulus intensity (µA)
e
Noradenaline in pancreatic LN (ng/mg of protein)
**
Sham
PNES

1

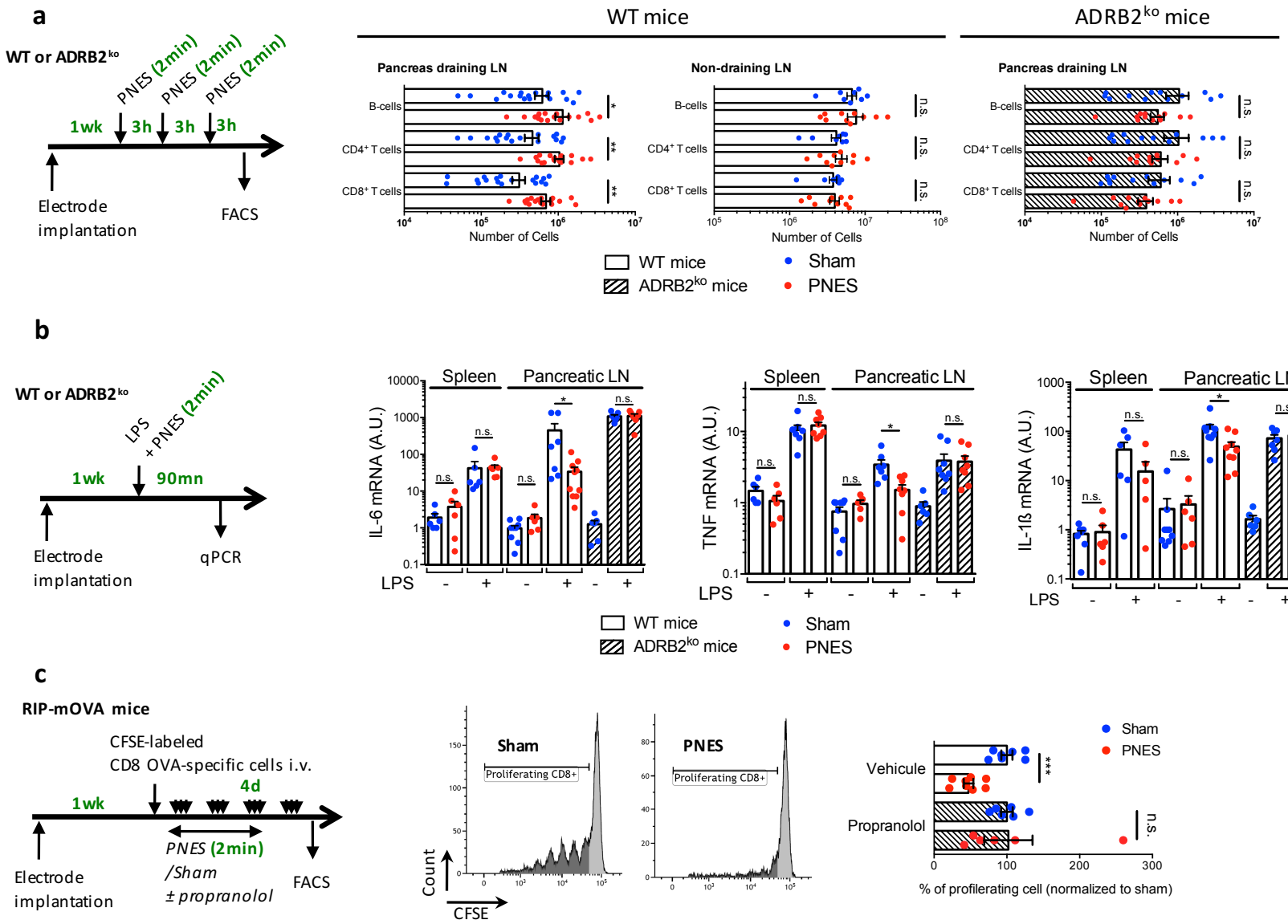
a
WT or ADRB2ko
PNES (2min)
PNES (2min)
PNES (2min)
1wk
3h
3h
3h
Electrode implantation
FACS
WT mice
ADRB2ko mice
Pancreas draining LN
Non-draining LN
Pancreas draining LN
B-cells
CD4+ T cells
CD8+ T cells
Number of Cells
n.s.
*
**
WT mice
ADRB2ko mice
Sham
PNES
b
WT or ADRB2ko
LPS
+PNES (2min)
1wk
90mn
Electrode implantation
qPCR
Spleen
Pancreatic LN
IL-6 mRNA (A.U.)
TNF mRNA (A.U.)
IL-1ß mRNA (A.U.)
LPS
WT mice
ADRB2ko mice
Sham
PNES
c
RIP-mOVA mice
CFSE-labeled
CD8 OVA-specific cells i.v.
4d
1wk
PNES (2min)
/Sham
± propranolol
Electrode implantation
FACS
Sham
PNES
Proliferating CD8+
Count
CFSE
Vehicule
Propranolol
Sham
PNES
% of profilerating cell (normalized to sham)

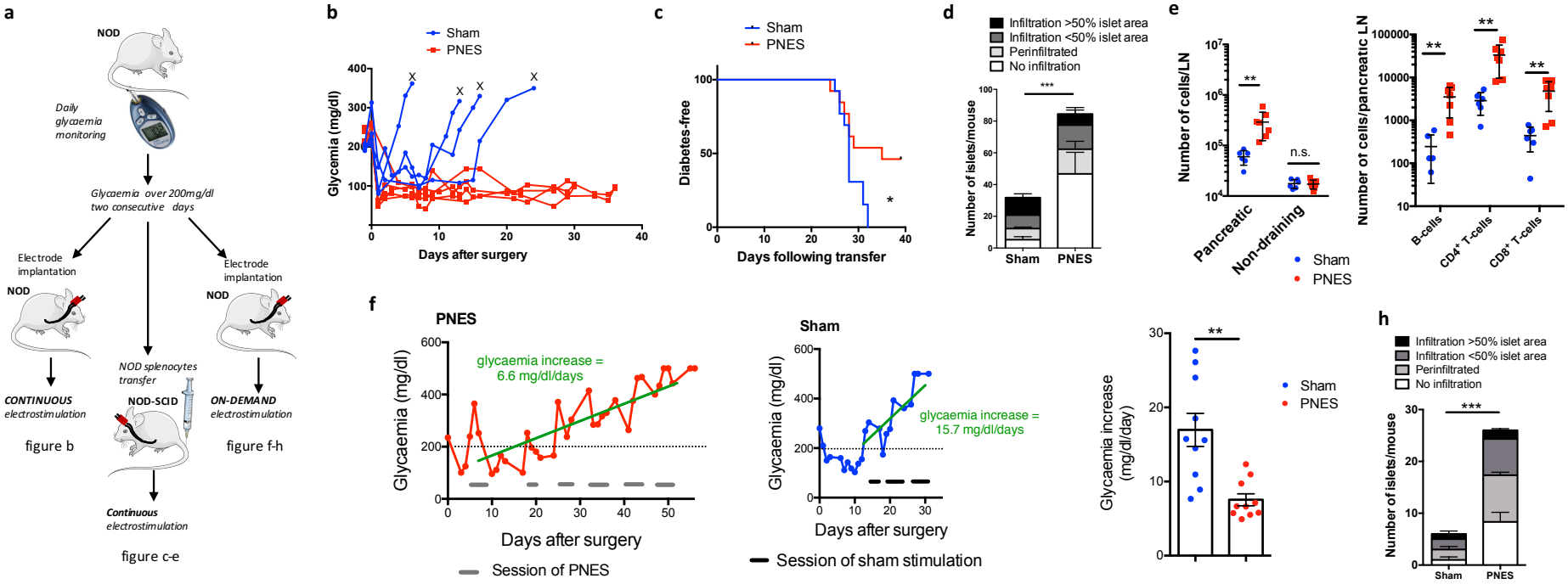
a
NOD
Daily glycaemia monitoring
Glycaemia over 200mg/dl two consecutive days
Electrode implantation
NOD
CONTINUOUS electrostimulation
figure b
NOD splenocytes transfer
NOD-SCID
Continuous electrostimulation
figure c-e
Electrode implantation
NOD
ON-DEMAND electrostimulation
figure f-h
b
Sham
PNES
Glycemia (mg/dl)
Days after surgery
c
Sham
PNES
Diabetes-free
Days following transfer
d
Infiltration >50% islet area
Infiltration <50% islet area
Perinfiltrated
No infiltration
Number of islets/mouse
Sham
PNES
e
Number of cells/LN
Pancreatic
Non-draining
n.s.
Sham
PNES
Number of cells/pancreatic LN
B-cells
CD4+ T-cells
CD8+ T-cells
f
PNES
glycaemia increase = 6.6 mg/dl/days
Glycaemia (mg/dl)
Days after surgery
Session of PNES
Sham
glycaemia increase = 15.7 mg/dl/days
Glycaemia (mg/dl)
Days after surgery
Session of sham stimulation
Glycaemia increase (mg/dl/day)
Sham
PNES
h
Infiltration >50% islet area
Infiltration <50% islet area
Perinfiltrated
No infiltration
Number of islets/mouse
Sham
PNES

1

Acknowledgements. We would like to thank Samah Rekima for technical assistance. This work was funded by a collaborative research grant from GSK Bioelectronics R&D. This work was also supported by the LABEX SIGNALIFE (#ANR-11-LABX-0028-01) and the FHU Oncoage.

Competing financial interest. A patent is pending on pancreatic nerve electrostimulation

Methods

Mice: All experiments were performed with female C57BL/6, NOD, NOD-SCID mice (Charles River), or RIP-mOVA[13], OT-I[14], ADRB2^{ko} [15] and tdTomato$^{TH\text{-}Cre}$ [16, 17] mice backcrossed onto the C57BL/6 background for at least 10 generations. Mice were housed on a 12 hours light/dark cycle (lights on/off at 7 am/7 pm) with food *ad libitum*. Mice were treated in accordance with our local Animal Care and Use Committee guidelines.

Electrodes and surgery: For studies in anaesthetized animals, mice were anaesthetized by an intraperitoneal injection of a mixture of ketamine (75 mg/kg) and xylazine (60 mg/kg) and a hook electrode was placed under the pancreatic nerve. For studies in conscious animals, mice were anaesthetized with isoflurane and the area around the right abdominal artery next to the kidney was exposed (**Suppl Fig. 1a**). One mm length 100 μm-sling micro-cuff electrodes (CorTec) were implanted onto the pancreatic nerve.

Recordings of CAP and FAP: After placing a hook electrode onto the pancreatic nerve and artery, platinum-iridium recording electrodes (Phymep) were placed onto the pancreatic nerve, pancreatic lymph node, pancreas tissue and liver for CAP recording using a wireless recording system (W8, Multi-Channel Systems). Ground/Reference wires were placed into the nearby tissue. For FAP, recordings were performed on explants from tdTomato$^{TH\text{-}Cre}$ that were placed in a recording chamber at room temperature (20-25°C) superfused with oxygenated artificial cerebrospinal fluid (ACSF) under a microscope (Zeiss). The pancreatic nerve was introduced into a suction-stimulating electrode stimulated with square pulses of 1 ms and intensities of 10-1500 μA. Recordings were made using pipettes made from borosilicate glass capillary (Hilgenberg) with resistance of 3–6 MW when filled with extracellular solution, placed near red fluorescent axons. Signals were amplified using an Axopatch 200B (Axon Instruments), digitized at 10kHz via an Digidata 3200 interface (Molecular devices) controlled by

pClamp10.0 software (Molecular Devices) and digitally filtered at 3KHz. CAP and FAP recordings were performed in a Faraday cage.

Electrostimulation: For studies on anaesthetized mice, Master-8 (A.M.P.I.), PlexStim V2.3 (Plexon) and STG 4002 stimulator (Multichannel system) were used respectively for CAP, pancreatic blood perfusion and FAP recording. For all studies in conscious animals, mice were placed in individual cage and connected to a PlexStim V2.3 (Plexon) or MAPS (Axonic) stimulator. Unless specified, the set-up of the electrostimulation were rectangular charged-balanced biphasic pulses with 450 μA pulse amplitude, 2 ms pulse width (positive and negative) at 10 Hz frequency for 2 minutes. In propranolol-treated groups, mice were injected intraperitoneally with a 5mg/kg dose, 30 min before electrostimulation.

Noradrenaline levels: Pancreatic LNs were harvested and snap-frozen in liquid nitrogen immediately after electostimulation. The organ was processed and noradernaline was measured by ELISA (DLD Diagnostika GmbH) via manufacturer recommandations.

Flow Cytometry: Single-cell suspensions were stained with anti-CD45 (clone 30F11), anti-CD3 (17A2), anti-CD4 (RM4-5), anti-CD8α (53-6.7), anti-CD19 (1D3). All antibodies are from BD Biosciences. Dead cells were excluded using 7-AAD staining. Data were acquired on SP6800 (Sony) flow cytometer and analyzed using Kaluza software.

RT-PCR: RNAs from pancreas were isolated *via* the manufacturer's instructions (miRNEasy micro kit, Quiagen), reverse transcribed using QuantiTect Reverse transcription kit (Quiagen) and amplicons were quantified SyberGreen Master Kit (Roche) and LightCycler 480 II (Roche). mRNAs cytokine expression were normalized to GAPDH using LightCycler software (Roche).

In vivo cross-priming assay: Cross-priming *in vivo* was assessed in Rip-mOVA mice. 10^7 of CFSE-labeled OT-I CD8+ T cells were injected intravenously to these mice at day 0. Between

day 1 and day 4, animals were electrostimulated or not (450 μA, 10 Hz, 2 minutes) 3 times a day (3 hours apart). On day 4, mice were sacrificed, pancreatic lymph node removed and $CD8^+$ proliferation was assessed by flow cytometry using SP6800 (Sony). Rip-mOVA mice were treated with propranolol (5mg/kg ip) 30mn before each stimulation.

Adoptive cell transfers in NOD-SCID: Recipients were adult 6-week-old NOD-SCID mice. Animals were injected intravenously with 5×10^6 splenocytes from overtly diabetic NOD mice.

Glycaemia follow-up: Glycaemia was monitored using a Free Style Papillon Vision (Abbott) taking a blood drop (<10 μl) from the tail. NOD and NOD-SCID mice were considered diabetic when glycaemia were over 250mg/dl for two successive days. To determine the increase slope of NOD mice linear regression to determine glycaemia including the first glycaemia time point over 200mg/dl and the 2 glycaemia time point exceeding 499mg/dl.

Laser speckle imaging: After anaesthesia, the pancreas tissue was exposed and placed about 30 cm below the Moor-FLPI laser speckle perfusion imager (Moor instruments Ltd.). Then the pancreatic blood perfusion images were saved and analyzed by the Image Review Program of Moor-FLPI-V2.0 software. The round region of interest (ROI) with the same area in each LSP image was selected for measuring the pancreatic blood perfusion.

Statistics: All findings shown have been reproduced in at least two independent experiments. Data are presented depending on their scale and distribution with arithmetic mean and standard deviation (mean ± s.e.m.). Normality was assessed using a Kolmogorov–Smirnov test. To compare independent measurements we used a t-test and Mann–Whitney U-test as appropriate. To compare dependent measurements we used a paired t-test. To compare more than two groups we used one-way ANOVA followed by Tukey's post hoc test. Diabetes-free curve is visualized by Kaplan–Meier curves and statistically compared by log-rank test. Statistical analysis was performed using GraphPad Prism v.6. The p values <0.05 were considered statistically

significant.

References

1. Birmingham, K. *et al.* Bioelectronic medicines: a research roadmap. *Nat. Rev. Drug Discov.* **13,** 399–400 (2014).
2. Herold, K. C. Restoring immune balance in type 1 diabetes. *Lancet Diabetes Endocrinol.* **1,** 261–263 (2013).
3. Padro, C. J. & Sanders, V. M. Neuroendocrine regulation of inflammation. *Semin. Immunol.* **26,** 357–368 (2014).
4. Duclaux, R., Mei, N. & Ranieri, F. Conduction velocity along the afferent vagal dendrites: a new type of fibre. *J. Physiol.* **260,** 487–495 (1976).
5. Fuentes, J. M. *et al.* General anesthesia delays the inflammatory response and increases survival for mice with endotoxic shock. *Clin. Vaccine Immunol. CVI* **13,** 281–288 (2006).
6. Lee, H. T., Emala, C. W., Joo, J. D. & Kim, M. Isoflurane improves survival and protects against renal and hepatic injury in murine septic peritonitis. *Shock Augusta Ga* **27,** 373–379 (2007).
7. Lee, H. T. *et al.* Isoflurane protects against renal ischemia and reperfusion injury and modulates leukocyte infiltration in mice. *Am. J. Physiol. Renal Physiol.* **293,** F713-722 (2007).
8. Christianson, S. W., Shultz, L. D. & Leiter, E. H. Adoptive transfer of diabetes into immunodeficient NOD-scid/scid mice. Relative contributions of CD4+ and CD8+ T-cells from diabetic versus prediabetic NOD.NON-Thy-1a donors. *Diabetes* **42,** 44–55 (1993).
9. Koopman, F. A. *et al.* Vagus nerve stimulation inhibits cytokine production and attenuates disease severity in rheumatoid arthritis. *Proc. Natl. Acad. Sci. U. S. A.* **113,** 8284–8289 (2016).

10. Bonaz, B. *et al.* Chronic vagus nerve stimulation in Crohn's disease: a 6-month follow-up pilot study. *Neurogastroenterol. Motil. Off. J. Eur. Gastrointest. Motil. Soc.* **28,** 948–953 (2016).
11. Hervé, J. *et al.* β2-Adrenoreceptor agonist inhibits antigen cross-presentation by dendritic cells. *J. Immunol. Baltim. Md 1950* **190,** 3163–3171 (2013).
12. Nakai, A., Hayano, Y., Furuta, F., Noda, M. & Suzuki, K. Control of lymphocyte egress from lymph nodes through β2-adrenergic receptors. *J. Exp. Med.* **211,** 2583–2598 (2014).
13. Kurts, C., Miller, J. F., Subramaniam, R. M., Carbone, F. R. & Heath, W. R. Major histocompatibility complex class I-restricted cross-presentation is biased towards high dose antigens and those released during cellular destruction. *J. Exp. Med.* **188,** 409–414 (1998).
14. Hogquist, K. A. *et al.* T cell receptor antagonist peptides induce positive selection. *Cell* **76,** 17–27 (1994).
15. Chruscinski, A. J. *et al.* Targeted disruption of the beta2 adrenergic receptor gene. *J. Biol. Chem.* **274,** 16694–16700 (1999).
16. Madisen, L. *et al.* A robust and high-throughput Cre reporting and characterization system for the whole mouse brain. *Nat. Neurosci.* **13,** 133–140 (2010).
17. Savitt, J. M., Jang, S. S., Mu, W., Dawson, V. L. & Dawson, T. M. Bcl-x is required for proper development of the mouse substantia nigra. *J. Neurosci. Off. J. Soc. Neurosci.* **25,** 6721–6728 (2005).

1